Clinical Cancer Research

Reversal of Warburg Effect and Reactivation of Oxidative Phosphorylation by Differential Inhibition of EGFR Signaling Pathways in Non–Small Cell Lung Cancer

Viviana De Rosa[1], Francesca Iommelli[1], Marcello Monti[2], Rosa Fonti[1], Giuseppina Votta[3], Maria Patrizia Stoppelli[3], and Silvana Del Vecchio[1,2]

Abstract

Purpose: One of the hallmarks of cancer cells is the excessive conversion of glucose to lactate under normoxic conditions, also known as the Warburg effect. Here, we tested whether the targeted inhibition of EGFR may revert this effect and reactivate mitochondrial oxidative phosphorylation in non–small cell lung cancer (NSCLC).

Experimental Design: Sensitive (HCC827) and resistant (H1975 and H1993) NSCLC cells were treated with a panel of EGFR or MET inhibitors, and then tested for changes of EGFR signaling, glycolytic cascade, and mitochondrial function. Silencing of key glycolytic enzymes was then performed with targeted siRNAs. Furthermore, tumor-bearing nude mice treated with EGFR inhibitors were evaluated with ^{18}F-FDG PET/CT and tumors were analyzed for glycolytic and mitochondrial proteins.

Results: Effective inhibition of EGFR signaling in NSCLC cells induced a dramatic reduction of hexokinase II (HKII) and phospho-pyruvate kinase M2 (p-PKM2, Tyr105) levels as well as an upregulation of mitochondrial complexes subunits (OXPHOS). Accordingly, a decreased lactate secretion and increased intracellular ATP levels were also observed in response to EGFR inhibitors. Downregulation of HKII and PKM2 by targeted siRNA transfection did not cause upregulation of OXPHOS but enhanced the effects of EGFR TKIs. Conversely, selective inhibition of AKT and ERK1/2 caused OXPHOS upregulation and glycolysis inhibition, respectively. Similar findings were obtained in tumors from animals treated with appropriate EGFR inhibitors.

Conclusions: Our findings indicate that EGFR inhibitors may reactivate oxidative phosphorylation of cancer cells and provide a mechanistic clue for the rational combination of agents targeting EGFR-dependent proliferation and glucose metabolism in cancer therapy. *Clin Cancer Res; 21(22); 5110–20. ©2015 AACR.*

Introduction

Oncogene-driven tumorigenesis implies the reprogramming of key regulatory steps of energy metabolism in cancer cells that become highly dependent on aerobic glycolysis rather than on mitochondrial oxidative phosphorylation (1, 2). The preferential conversion of glucose to lactic acid in cancer cells under normoxic conditions, also known as Warburg effect (3, 4), is nowadays considered a hallmark of cancer. Although energetically ineffective, glycolysis is reported to support the uncontrolled growth and survival of cancer cells by favoring the generation of macromolecular building blocks such as nucleotides, amino acids, and lipids through alternative biosynthetic pathways (5, 6).

Many oncogenic signaling pathways were reported to cause the shift from oxidative phosphorylation to aerobic glycolysis in cancer cells (7, 8). In particular, aberrant signaling from EGFR through the PI3K–AKT or RAS–MAPK pathways was reported to modulate the expression of a pool of genes encoding glucose transporters and most glycolytic enzymes (1, 9).

EGFR is recognized as an oncogene driver in non–small cell lung cancer (NSCLC) because activating mutations in the kinase domain of EGFR cause an enhanced EGFR tyrosine kinase activity and a persistent activation of downstream signaling pathways that, in turn, drive oncogenesis and tumor progression (10). Previous studies identified indeed the presence of activating mutations in the kinase domain of EGFR as a major determinant of effective tumor response of NSCLC to gefitinib or erlotinib (11–14). However, despite initial response to treatment, virtually all NSCLC patients develop resistance to EGFR TKIs due to the occurrence of T790M secondary mutations in EGFR (15, 16) or to the amplification of MET receptor tyrosine kinase (17) and several compounds have been developed and tested to overcome EGFR TKIs resistance (18–20).

We hypothesized that by inhibiting EGFR signaling, to which tumor cells are addicted, may cause in addition to growth arrest and apoptosis, an early metabolic switch from aerobic glycolysis to mitochondrial oxidative phosphorylation. Therefore, the aim of the present study was to test whether the efficient inhibition of EGFR pathways in EGFR-driven NSCLCs may revert the Warburg effect and reactivate mitochondrial oxidative phosphorylation both *in vitro* and *in vivo*.

[1]Institute of Biostructures and Bioimages, National Research Council, Naples, Italy. [2]Department of Advanced Biomedical Sciences, University of Naples Federico II, Naples, Italy. [3]Institute of Genetics and Biophysics, National Research Council, Naples, Italy.

Corresponding Author: Silvana Del Vecchio, University of Naples Federico II, Via Pansini 5, Edificio 10, 80131 Napoli, Italy. Phone: 39-081-746-3307; Fax: 39-081-545-7081; E-mail: delvecc@unina.it

doi: 10.1158/1078-0432.CCR-15-0375

AACR

Translational Relevance

Energy metabolism of cancer cells is highly dependent on aerobic glycolysis rather than on mitochondrial oxidative phosphorylation and many oncogenes, including EGFR, may promote the acquisition of the glycolytic phenotype. Here, we report that targeted inhibition of EGFR pathways may revert aerobic glycolysis and reactivate mitochondrial oxidative phosphorylation in non–small cell lung cancer through the concerted downregulation of hexokinase II (HKII) and phospho-pyruvate kinase M2 (p-PKM2) and upregulation of OXPHOS. Suppression of HKII and PKM2 levels by RNA silencing does not affect OXPHOS levels, but enhances the effects of EGFR inhibitors. Conversely, selective inhibition of AKT and ERK1/2 leads to OXPHOS upregulation and aerobic glycolysis inhibition, respectively. The translational relevance of our study is to show that EGFR inhibitors may reactivate oxidative phosphorylation of cancer cells and provide a mechanistic clue for the rational combination of agents targeting EGFR-dependent proliferation and glucose metabolism in cancer therapy.

To this end, EGFR-driven H1975 and HCC827 NSCLC cells bearing or not T790M mutation were treated with WZ4002, a specific inhibitor of $EGFR^{T790M}$, and erlotinib so that differential changes of glycolytic cascade and glucose metabolism could be tested in the same cellular context after treatment with efficient or inefficient inhibitors. A similar approach was adopted in H1993 NSCLC cells bearing wild-type EGFR and MET amplification using erlotinib and MET inhibitors such as PHA-665,752 or crizotinib. Finally, our hypothesis was tested in untreated and treated nude mice bearing H1975 and H1993 xenografts.

Materials and Methods

Cell lines and treatment

Three NSCLC cell lines were obtained from and authenticated by the ATCC. In particular, H1975 cells bear an activating point mutation in exon 21 (L858R) and also harbor the T790M mutation in the kinase domain of EGFR (15, 16). Despite the T790M-mediated resistance, H1975 remain EGFR driven. HCC827 cells are highly responsive to erlotinib due to the presence of an activating deletion of exon 19 (delE746_A750) of *EGFR* (21). H1993 cells are reported to have a high level of *MET* gene amplification (15 copy numbers; refs. 22, 23) and wild-type EGFR, thus showing resistance to erlotinib (17). HCC827 cells served as control for both resistant cell lines because they also express high levels of MET protein on their plasma membrane but do not have *MET* gene amplification (17, 22). All cells were grown in RPMI medium supplemented 10% FBS, 100 IU/mL penicillin and 50 μg/mL streptomycin in a humidified incubator with 5% CO_2 at 37°C.

Cells were treated with 1 μmol/L erlotinib, 0.1 or 1 μmol/L WZ4002 (Selleck Chemicals), an irreversible EGFR TKI that binds T790M-harboring receptor, or 1 μmol/L PHA-665,752 (Selleck Chemicals), a selective MET inhibitor, in serum-free RPMI for the indicated time as previously described (18, 19). Parallel experiments were performed by treating cells with increasing concentrations of AKT inhibitor, wortmannin (Biaffin GmbH & Co KG, Germany), and MAP kinase (ERK1/2) inhibitor, U0126 (Calbiochem).

Immunoblotting analysis

Whole-cell lysates and membrane fractions were prepared as previously described (19, 24). Briefly untreated and treated cells were lysed, homogenized, and centrifuged at 13,000 × *g* at 4°C for 20 minutes to obtain whole-cell lysates. Membrane fractions were prepared by resuspending cells in an isotonic buffer followed by homogenization and centrifugation at 800 × *g* at 4°C for 10 minutes (24). The supernatant was ultracentrifuged at 46,000 × *g* at 4°C for 45 minutes and the resulting pellet containing the membrane fraction was resuspended in HEPES buffer 50 mmol/L.

Western blot analysis of proteins from different lysates was performed using a standard procedure. Antibodies used for western blotting included mouse monoclonal antibodies against phospho-EGFR (Cell Signaling Technology; 0.1 mg/mL), p42/44 MAP kinase (ERK1/2; Cell Signaling Technology; 0.1 mg/mL), MET (25H2; Cell Signaling Technology; 0.1 mg/mL), α-tubulin (Sigma; 1 μg/mL), β-actin (Sigma; 1 μg/mL); the OXPHOS cocktail of mouse polyclonal antibodies (Mitoscience, Eugene, OR; 1:1,000) targets the following proteins: 20 kD subunit of Complex I (20 kD), COX II of Complex IV (22 kD), 30 kD Ip subunit of Complex II (30 kD), core 2 of Complex III (∼ 50 kD), and F1α (ATP synthase) of Complex V (∼ 60 kD); rabbit monoclonal antibody against PKM2 (Cell Signaling Technology; 0.1 mg/mL); rabbit polyclonal antibodies against PKM1 (Abgent; 1:1,000), EGFR (Santa Cruz Biotechnology; 1:1,000), phospho-AKT (Ser 473; Santa Cruz Biotechnology; 1:1,000), Hexokinase I (Cell Signaling Technology; 1:1,000), Hexokinase II (Cell Signaling Technology; 1:1,000), phospho-PKM2 (Tyr105; Cell Signaling Technology; 1:1,000), phospho-p42/44 MAP kinase (ERK1/2; Cell Signaling Technology; 1:1,000), phospho-MET (Tyr 1234/1235; Cell Signaling Technology; 1:1,000), AKT (Cell Signaling Technology; 1:1,000), Cyclin D1 (Cell Signaling Technology; 1:1,000), Na^+,K^+-ATPase, (Cell Signaling Technology; 1:1,000), GLUT1 (Abcam; 1:1,000), GLUT3 (Abcam; 1:1,000), and PGC-1α (Abcam; 1:1,000). A commercially available ECL kit (GE Healthcare) was used to reveal the reaction.

Quantitative real-time PCR analysis

Total RNA was extracted from untreated and treated H1975 cells using the RNeasy Mini Kit (Qiagen) following the manufacturer's instructions. RNA (1 μg) was reverse transcribed to cDNA using oligonucleotides and Superscript III (Invitrogen). Samples of cDNA were then subjected to PCR analysis using the 7900HT Fast Real-Time PCR System (Applied Biosystems) and SYBR Green dye (Applied Biosystems) for quantitation. The expression of *GLUT1*, *GLUT3*, *HKI*, *HKII*, *PKM1*, *PKM2*, *LDH-A*, and actin, as reference gene, was analyzed and the specific synthesized primers were purchased from Primm. A standard RT-PCR protocol was used. Threshold cycle (C_t) values were automatically calculated for each sample and used to determine the relative expression of target genes compared with the reference gene in all samples by the $2^{-\Delta\Delta Ct}$ method. Data were expressed as relative mRNA level of each treated sample compared with the corresponding untreated control. Four independent experiments were performed and each sample was analyzed in triplicates.

^{18}F-FDG uptake, glucose consumption, lactate secretion, and intracellular ATP in cultured tumor cells

Cells were seeded in 12-well flat-bottomed plates at a density of 1.5×10^5 cells per well, and then treated with EGFR TKIs or MET inhibitor at the indicated concentration in serum-free RPMI for 48 hours. Cells were incubated with 2 μCi/mL of ^{18}F-Fluorodeoxyglucose (^{18}F-FDG) in 500 μL of glucose-free medium for 60 minutes at 37°C in triplicates. After washing, they were lysed with 1 mol/L NaOH and cell-associated radioactivity was determined using a gamma counter (Packard). The uptake of ^{18}F-FDG in untreated and treated cells was determined as a percentage of added radioactivity and normalized for 10^6 cells. At least three independent assays were performed for each cell line and for each treatment. Finally, data were expressed considering the corresponding untreated cells as 100%.

In parallel experiments untreated and treated cells were analyzed for glucose and lactate levels in the conditioned media and for intracellular ATP levels. Briefly after 48 hours treatment with EGFR TKIs or MET inhibitor, conditioned media were removed, centrifuged at 13,000 × *g* at 4°C for 10 minutes and then assayed for glucose and lactate concentrations using the Glucose Assay Kit (Sigma-Aldrich) and the Lactate Assay Kit (Sigma-Aldrich) following the manufacturer's instructions. Untreated and treated cells were simultaneously subjected to intracellular ATP determination using the ATPlite Luminescence Assay (PerkinElmer) following the manufacturer's instructions. Briefly, cells were lysed, incubated with the ATP reaction mixture for 5 minutes, and then subjected to luminescence measurements. Absolute glucose, lactate, and ATP levels were calculated from the corresponding standard curve and normalized to 10^6 cells. Similarly citrate and malate levels were determined in untreated and treated cells using the Citrate and Malate Assay Kit (Sigma-Aldrich).

Oxygen consumption and extracellular acidification rates

The oxygen consumption rate (OCR) and extracellular acidification rate (ECAR) were determined using the Seahorse Extracellular Flux Analyzer (XF-96; Seahorse Bioscience). Briefly, H1975 cells were seeded at 10,000 cells per well on XF 96-well microplates and allowed to attach overnight. Cells were then treated with 1 μmol/L WZ4002 or vehicle for 48 hours. OCR was measured in basal conditions and after the subsequent addition of 5 μmol/L oligomycin, 1.5 μmol/L carbonylcyanide-4-(trifluoromethoxy)-phenylhydrazone (FCCP), and 1 μmol/L rotenone/antimycin A. ECAR was simultaneously measured in basal conditions and after the subsequent addition of 10 mmol/L glucose, 5 μmol/L oligomycin, and 100 mmol/L 2-deoxyglucose. OCR and ECAR were monitored over time and each cycle consisted of 3 minutes mixing, 3 minutes waiting, and 3 minutes measuring. Data were normalized for 10^6 cells and expressed as pmol/min and mpH/min, respectively.

RNA interference

GLUT3, HKII, and PKM2-targeted siRNA pools (ON-TARGETplus SMARTpool) and control non-targeting siRNA pool (scrambled) were purchased from Dharmacon, Inc. and used according to the manufacturer's instructions. Briefly, H1975 cells were plated (2×10^5) and allowed to attach for 24 hours. Then cells were transfected with 100 nmol/L siRNAs using Dharmafect reagent (Dharmacon) and after 24 hours cells were treated with 1 μmol/L WZ4002 or vehicle for 48 hours, and then lysed for Western blot analysis.

Treatment of animal tumor models and imaging studies

Female BALB/c (nu/nu) mice, 6-week-old, weighing 15 to 20 g were purchased from Charles River Laboratories. All animal experimental procedures were approved by the Italian Ministry of Health-Animal Welfare Direction (protocol no. DGSAF21940-A-16/11/2013). H1975 and H1993 cells ($5–10 \times 10^6$) were resuspended in 200 μL RPMI medium and injected s.c. into the flank of nude mice (groups of 4 mice, $n = 3$ experiments). When tumors reached a mean volume of approximately 100 mm^3, animals were treated daily for 3 days by oral gavage with 50 mg/kg of WZ4002, erlotinib, crizotinib, or vehicle as previously described (19). In addition animals ($n = 3$ for each cell line) treated with the efficient inhibitor or vehicle underwent a baseline and a post-treatment scan using a small-animal Positron Emission Tomography/Computerized Tomography (PET/CT) scanner (eXplore Vista Pre-Clinical PET Scanner GE Healthcare). After fasting for 8 hours, animals received 200 μCi (7.4 MBq) of ^{18}F-FDG by i.v. injection through the tail vein. Animals were anesthetized using 2% isoflurane and then subjected to PET/CT scan at 60 minutes after injection. Body temperature of the animals was held constant during tracer biodistribution and imaging studies by heating pad or heat lamp. One bed position, including the tumor, was scanned and CT images were acquired with the X-ray source set at 35 kVp and 200 μA for 10 minutes followed by PET images acquisition for 20 minutes.

Levels of HKII, p-PKM2 Tyr105, total PKM2, and OXPHOS in excised tumors

After 3 days of treatment tumors were surgically removed, immediately frozen in liquid nitrogen and stored at −80°C until used. Tumor samples obtained from animals treated or not with 50 mg/kg WZ4002, erlotinib, or crizotinib were homogenized on ice in RIPA lysis buffer with protease and phosphatase inhibitors (Sigma-Aldrich) using a dounce homogenizer followed by passages through a 26-gauge needle. The suspension was clarified by centrifugation at 13,000 × *g* for 30 minutes at 4°C and subjected to Western blot analysis.

Statistical analysis

Statistical analysis was done using the software MedCalc for Windows, version 10.3.2.0 (MedCalc Software). An unpaired and paired Student *t* test was used when appropriate to compare means. Differences between means were considered statistically significant for $P < 0.05$.

Results

HKII and p-PKM2 Tyr105 downregulation by efficient inhibition of EGFR signaling in sensitive and resistant NSCLC cells

To investigate the effects of EGFR tyrosine kinase activity on glucose metabolism of NSCLC cells, three human lung cancer cell lines were selected, based on their different sensitivity to EGFR TKIs. The NSCLC H1975 and HCC827 cell lines were exposed to the EGFR TKIs erlotinib or WZ4002, a specific inhibitor of EGFR^{T790M}. Conversely, the H1993 cell line, bearing *MET* gene amplification, was treated either with erlotinib or with the MET inhibitor PHA-665,752. In all cases, the levels of p-EGFR, and relative p-AKT, p-ERK1/2 and cyclin D1 downstream mediators were analyzed. Cell exposure to increasing concentration of WZ4002 caused a concomitant decrease of p-EGFR, p-AKT,

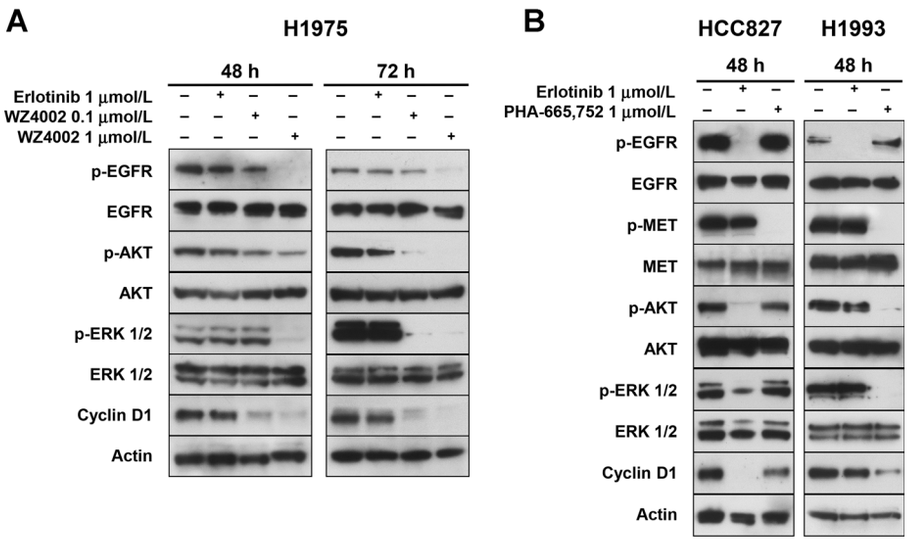

Figure 1.
Efficient inhibition of EGFR signaling in sensitive and resistant NSCLC cells. Representative Western blot analysis of whole-cell lysates from NSCLC H1975 cells treated with 1 μmol/L erlotinib, 0.1 or 1 μmol/L WZ4002, a specific inhibitor of $EGFR^{T790M}$, for 48 and 72 hours (A) and NSCLC HCC827 and H1993 cells treated with 1 μmol/L erlotinib or PHA-665,752, a specific MET inhibitor, for 48 hours (B). Actin served to ensure equal loading.

p-ERK1/2, and cyclin D1 levels in H1975 cells at both 48 and 72 hours, whereas no significant changes were observed in the same cells exposed to erlotinib (Fig. 1A). In contrast, HCC827 cells did respond to erlotinib and not to PHA-665,752 (Fig. 1B). As expected H1993 were sensitive to PHA-665,752 and showed a concomitant decrease of p-MET, p-AKT, p-ERK1/2, and cyclin D1 levels. Despite the strong inhibition of EGFR phosphorylation by erlotinib, only a slight reduction of p-AKT and cyclin D1 was observed in erlotinib-treated H1993 cells.

Next, we investigated the effects of cell exposure to the different inhibitors on the levels of relevant glucose transporters and glycolytic enzymes. Concomitant changes of GLUT1, GLUT3, HKI, HKII, PKM1, and PKM2 protein levels were assessed in H1975, HCC827, and H1993 cells treated with WZ4002, erlotinib, or PHA-665,752 for the indicated time. As a result, the protein levels of GLUT1, HKI, PKM1, and PKM2 remained substantially unchanged in all cell lines (Fig. 2A and 2B). However, in H1975 cells, WZ4002 caused a strong dose-dependent reduction of HKII levels. A similar reduction of HKII was observed in HCC827 and H1993 cells after 48 hours treatment with erlotinib or PHA-665,752, respectively, indicating that HKII levels are downregulated in all cell lines exposed to efficient inhibitors.

Interestingly, an increase of GLUT3 levels were observed in whole-cell lysates after 72 hours treatment of H1975 with WZ4002 or following treatment of H1993 cells with PHA-665,752. Because other authors reported GLUT3 translocation from the plasma membrane to the cytosol in response to EGFR inhibition (25), we tested GLUT3 levels in membrane fractions of H1975 cells treated with EGFR TKIs. A decrease of GLUT3 levels in membrane fractions was observed after 72 hours treatment with WZ4002 (Fig. 2C), indicating the translocation of the glucose transporter from the plasma membrane into the cytosol of treated cells.

In agreement with these findings mRNA levels of GLUT3 were significantly reduced in a dose-dependent manner after treatment of H1975 cells with WZ4002 ($P < 001$; Fig. 2D). Conversely, no significant changes of the mRNA levels of GLUT1, HKI, PKM1, and PKM2 were observed in treated cells. In agreement with the protein expression data, mRNA levels of HKII were significantly reduced ($P < 0.01$) at high-dose treatment with WZ4002, suggesting that downregulation of HKII in response to EGFR inhibition occurs at transcriptional level.

Because posttranslational modifications of PKM2 such as phosphorylation at Tyr105 regulate PKM2 activity by modulating the balance between active tetrameric and inactive dimeric forms of this enzyme (26, 27), we tested the levels of phosphorylated PKM2 at Tyr105 (p-PKM2 Tyr105) in whole-cell lysates of H1975 cells exposed to WZ4002 for 48 and 72 hours. A dose-dependent reduction of p-PKM2 Tyr105 levels was observed in response to WZ4002 treatment as compared with untreated and erlotinib-treated controls (Fig. 3A). A similar reduction of p-PKM2 Tyr105 levels was observed in HCC827 cells treated with erlotinib but not with PHA-665,752. In H1993 cells, levels of p-PKM2 Tyr105 were strongly reduced after treatment with PHA-665,752 and only slightly reduced in response to erlotinib treatment (Fig. 3B).

OXPHOS upregulation in response to EGFR TKIs

The reduction of p-PKM2 Tyr105 levels is reported to promote the active tetrameric form of the enzyme (27, 28), thus enhancing the conversion of phosphoenolpyruvate to pyruvate that, in turn, can be subjected either to lactate conversion or to oxidative phosphorylation. Therefore, we tested the expression of specific mitochondrial complexes subunits (OXPHOS) in untreated and treated cells. Figure 3C shows that treatment of H1975 cells with 1 μmol/L WZ4002 increased the expression of all subunits tested except ATP5A of complex V whose levels remained constantly high in untreated and treated cells. An enhanced expression of subunits of complexes II, III, IV, and V was also observed in HCC827 cells exposed to erlotinib (Fig. 3D). NDUFB8 subunit of complex I was undetectable in untreated and treated HCC827 cells that are reported to bear mtDNA mutations in complex I subunits causing an altered assembly of complex I and mitochondrial dysfunction (29). In H1993 cells treated with 1 μmol/L PHA-665,752, a strong upregulation of all subunits tested was found as compared with untreated control cells whereas a slight increase of subunits of complex I, II, and IV was observed in the same cell line exposed to erlotinib. These findings taken together, raise the

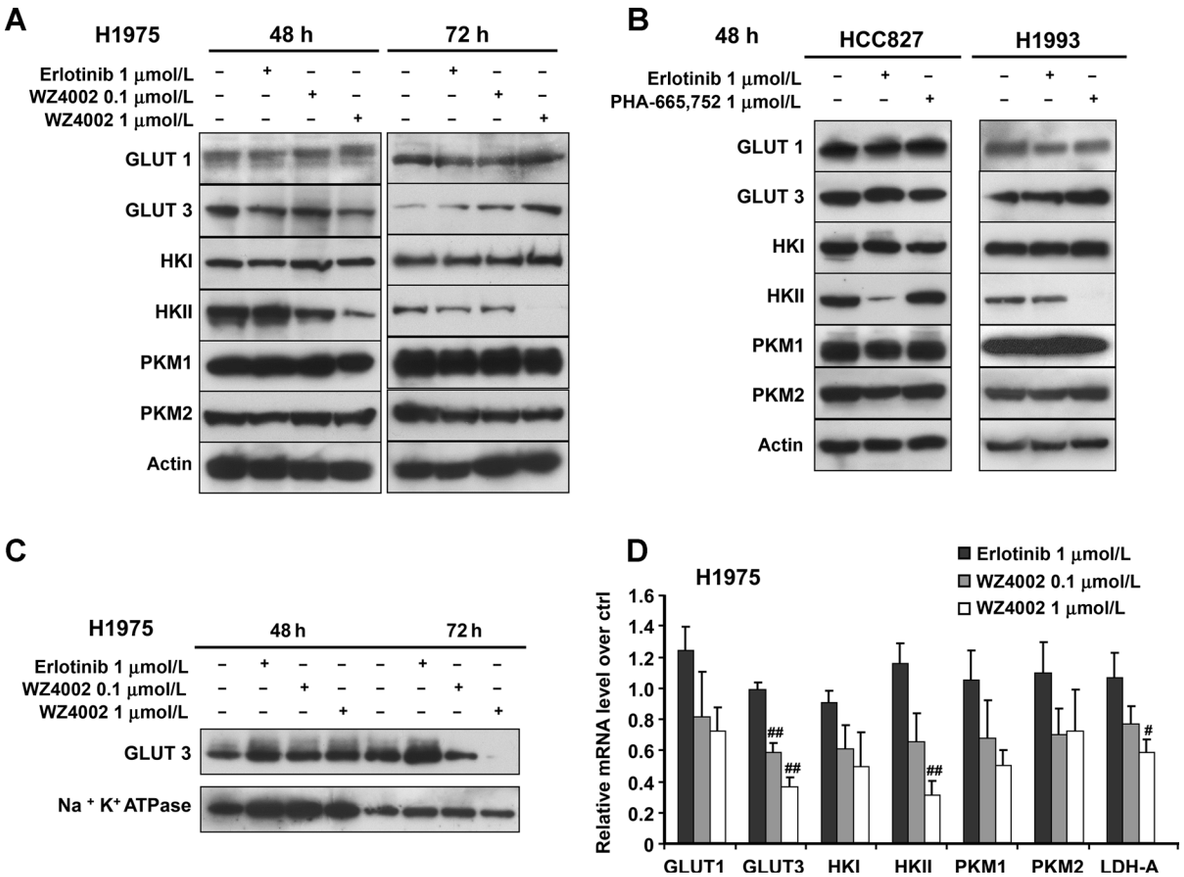

Figure 2.
Protein and mRNA levels of relevant glucose transporters and glycolytic enzymes in NSCLC cells exposed to efficient EGFR inhibitors. A, protein levels of GLUT1, GLUT3, HKI, HKII, PKM1, and PKM2 in whole-cell lysates from H1975 cells exposed to 1 μmol/L erlotinib, 0.1 or 1 μmol/L WZ4002 for 48 and 72 hours. B, levels of the same proteins in whole-cell lysates from HCC827 and H1993 cells treated with 1 μmol/L erlotinib or PHA-665,752 for 48 hours. C, GLUT3 levels in membrane fractions from H1975 cells exposed to 1 μmol/L erlotinib, 0.1 or 1 μmol/L WZ4002 for 48 and 72 hours. Actin and Na^+/K^+-ATPase served to ensure equal loading of samples from whole-cell lysates and membrane fractions, respectively. D, mRNA levels of GLUT1, GLUT3, HKI, HKII, PKM1, PKM2, and LDH-A by RT-PCR in H1975 cells exposed to erlotinib, WZ4002 or vehicle at the indicated doses for 48 hours. Significant differences with $^{\#}$, $P < 0.05$ and $^{\#\#}$, $P < 0.01$.

possibility that mitochondrial respiration is indeed upregulated by cell exposure to the selected inhibitors.

Reactivation of oxidative phosphorylation by EGFR signaling inhibition

To test whether the increased levels of mitochondrial complexes subunits were associated with a functional reactivation of oxidative phosphorylation and reversal of aerobic glycolysis, we assessed the uptake and consumption of glucose along with the intracellular ATP and lactate levels. Figure 4A shows that ^{18}F-FDG uptake was significantly reduced ($-61\% \pm 10\%$) in H1975 cells after treatment with 1 μmol/L WZ4002 compared with untreated ($P = 0.02$) and erlotinib-treated ($P = 0.02$) cells. Similarly, H1993 cells showed a significant reduction of ^{18}F-FDG uptake ($-71\% \pm 11\%$) in response to 1 μmol/L PHA-665,752 as compared with untreated cells ($P = 0.04$). When exposed to 1 μmol/L erlotinib, H1993 cells showed a moderate ($-35\% \pm 30\%$) but not statistically significant ($P = 0.41$) decrease of ^{18}F-FDG uptake as compared with untreated cells. In agreement with these findings, residual glucose levels in H1975 and H1993 conditioned media were significantly increased as compared with untreated controls ($P < 0.0001$) after 48 hours of treatment with WZ4002 (up to 4-fold) and PHA-665,752 (up to 3-fold), respectively (Fig. 4B). Interestingly, in H1993 conditioned media, a slight but significant increase (1.3-fold, $P = 0.004$) of extracellular glucose levels was observed in response to 48 hours treatment with erlotinib. These data consistently indicate that both glucose uptake and consumption were reduced in H1975 and H1993 cells in response to inhibition of EGFR signaling.

Parallel determination of intracellular ATP levels showed that 48 hours treatment with 1 μmol/L WZ4002 caused a statistically significant 2.3-fold increase of ATP levels in H1975 cells ($P < 0.0001$; Fig. 4C). Similarly, a 2.7- and 1.7-fold significant increase of ATP levels was found in H1993 cells exposed to PHA-665,752 ($P = 0.001$) and erlotinib ($P = 0.011$), respectively, as compared with untreated cells. Conversely, a statistically significant 2-fold decrease of lactate levels was found in conditioned media of H1975 cells after 48 hours treatment with 1 μmol/L WZ4002 as compared with untreated controls ($P < 0.0001$; Fig. 4D). Lactate levels in H1993 conditioned media were reduced by 2.8- and 1.7-fold after treatment with PHA-665,752 ($P < 0.0001$) and erlotinib ($P = 0.0005$), respectively, as compared with untreated controls.

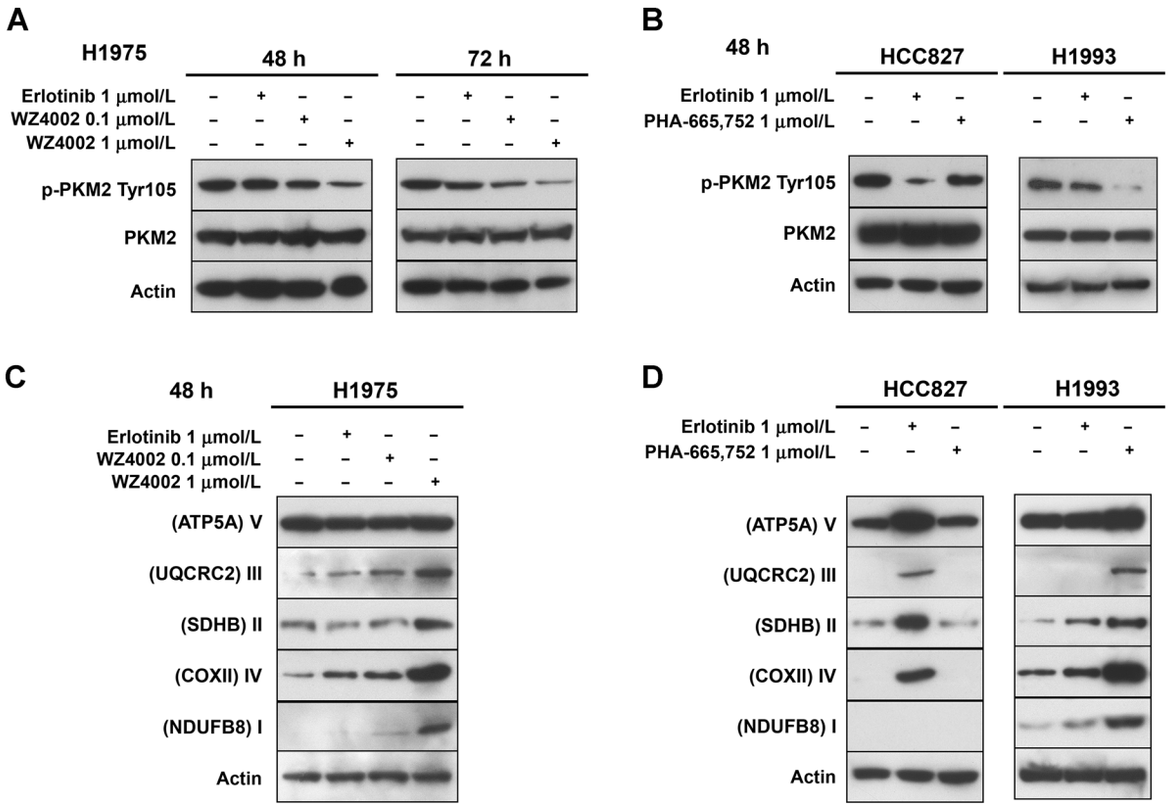

Figure 3.
Levels of p-PKM2 Tyr105 and OXPHOS in response to EGFR inhibitors. Levels of p-PKM2 Tyr105 in whole-cell lysates from H1975 cells treated with 1 μmol/L erlotinib, 0.1 and 1 μmol/L WZ4002 for 48 and 72 hour (A) or from HCC827 and H1993 cells treated with 1 μmol/L erlotinib or PHA-665,752 for 48 hours (B). C, levels of OXPHOS in whole cell lysates from H1975 cells exposed to 1 μmol/L erlotinib, 0.1 or 1 μmol/L WZ4002 and from HCC827 and H1993 cells treated with 1 μmol/L erlotinib or PHA-665,752 for 48 hours (D). Actin served to ensure equal loading.

The reduced glucose uptake and consumption along with the inverse relationship between lactate secretion and intracellular ATP production support the evidence that mitochondrial respiration is indeed reactivated following treatment with efficient inhibitors. To further confirm functional reactivation of oxidative phosphorylation, OCR and ECAR were measured in untreated and treated H1975 cells over time and a significant OCR increase ($P < 0.001$) and a concomitant ECAR decrease ($P < 0.05$) were found after inhibition of ATP synthase with oligomycin (Fig. 4E), whereas no significant differences were found in the other key parameters of mitochondrial respiration and glycolysis. Finally, citrate levels increased by 2.4-fold ($P < 0.05$) and 1.6-fold ($P < 0.05$) in treated H1975 and H1993 cells (Fig. 4F), respectively, whereas no significant changes of malate levels were found in the same samples.

Targeted mRNA silencing of HKII and PKM2

To test the existence of a cause-effect relationship between the reduced levels of relevant glycolytic enzymes and upregulation of mitochondrial complexes, silencing of HKII and PKM2 mRNAs was accomplished with targeted or scrambled siRNAs. Fig. 5A shows the resulting levels of HKII, PKM2, and OXPHOS in transiently transfected cells in the absence or presence of EGFR inhibitor. Silencing HKII was not associated with any changes of p-PKM2 Tyr105, total PKM2, and OXPHOS in the absence of EGFR inhibitor. The downregulation of PKM2 levels resulted in the suppression of its phosphorylated form and HKII levels in the absence of EGFR inhibitor, whereas no OXPHOS upregulation was observed. The addition of WZ4002 to both targeted siRNA-transfected cells caused a stronger OXPHOS upregulation as compared with scrambled siRNA-transfected cells exposed to EGFR inhibitor. Silencing GLUT3 did not cause any significant changes of HKII, p-PKM2 Tyr105, total PKM2, and OXPHOS levels as compared with controls (data not shown). Taken together, these findings indicate that the upregulation of OXPHOS is neither dependent on HKII nor on PKM2 suppression and does not compensate for glycolysis inhibition. More importantly, the downregulation of these enzymes enhances the effect of EGFR TKIs on the upregulation of OXPHOS, indicating that the inhibition of EGFR signaling pathways is required for reactivation of oxidative phosphorylation.

Differential regulation of aerobic glycolysis and OXPHOS by ERK1/2 and AKT pathways

Then, we tested whether selective inhibition of AKT or ERK1/2 pathways by wortmannin and U0126, respectively, could affect levels of HKII, p-PKM2 Tyr105, total PKM2, and OXPHOS. When H1975 cells were exposed to increasing concentration of AKT inhibitor, a dose-dependent increase of OXPHOS levels (subunits I-IV) was observed (Fig. 5B) whereas no changes of HKII and

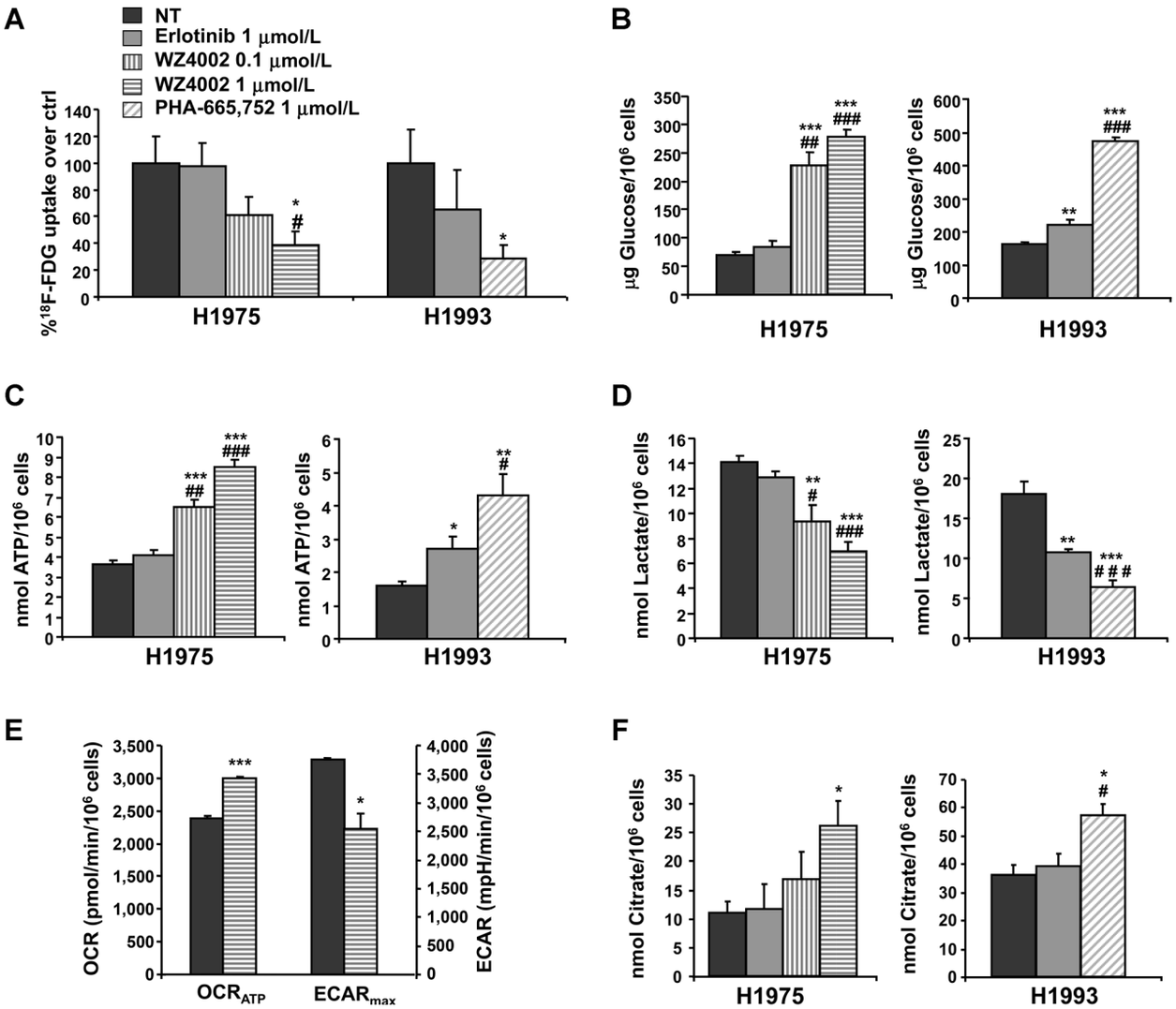

Figure 4.

Inhibition of aerobic glycolysis and reactivation of oxidative phosphorylation in H1975 and H1993 cells exposed to EGFR TKIs. NSCLC cells were treated for 48 hours with erlotinib, WZ4002 or PHA-665,752 at the indicated doses. A, untreated and treated cells were then incubated with ^{18}F-FDG for 1 hour. After washing, the uptake of ^{18}F-FDG was determined as a percentage of added radioactivity and normalized for 10^6 cells. Data are expressed considering the corresponding untreated cells as 100%. B, residual glucose levels were measured in conditioned media from untreated and treated cells. Data are expressed as μg of glucose normalized to 10^6 cells. C, intracellular ATP levels were determined in lysates of untreated and treated cells and expressed as nmol of ATP normalized to 10^6 cells. D, lactate levels were measured in conditioned media of untreated and treated cells and expressed as nmol of secreted lactate normalized to 10^6 cells. E, concomitant OCR and ECAR measurements were obtained after inhibition of ATP synthase with oligomycin (OCR_{ATP} and $ECAR_{max}$) in H1975 cells treated or not with 1 μmol/L WZ4002 for 48 hours and normalized to 10^6 cells. OCR and ECAR scales are on the left and right *y*-axis, respectively. F, citrate levels were determined in untreated and treated cells and expressed as nmol of citrate normalized to 10^6 cells; data, as mean ± SE. Significant differences versus untreated control with *, $P < 0.05$; **, $P < 0.01$; and ***, $P < 0.001$; significant differences versus erlotinib-treated cells with #, $P < 0.05$; ##, $P < 0.01$; and ###, $P < 0.001$.

p-PKM2 Tyr105 levels were observed. Conversely, treatment with ERK1/2 inhibitor caused a dose-dependent decrease of HKII and p-PKM2 Tyr105 levels whereas no changes of OXPHOS levels were observed in treated cells (Fig. 5C). These findings indicate that OXPHOS expression is modulated by AKT-mediated signaling whereas HKII and p-PKM2 Tyr105 levels are regulated by ERK1/2-mediated signaling. Therefore, the fine tuning of both pathways regulates in a concerted manner the inhibition of aerobic glycolysis and the reactivation of mitochondrial respiration. Finally, because PGC-1α is a key regulator of mitochondrial biogenesis, its protein levels were tested in response to treatment and a dose-dependent upregulation of PGC-1α was found in H1975 cells upon exposure to WZ4002 (Fig. 5D).

Reversal of Warburg effect and reactivation of oxidative phosphorylation by EGFR TKIs in tumor-bearing mice

Finally, we investigated the effects of EGFR inhibition in nude mice bearing H1975 and H1993 xenografts that were treated with 50 mg/kg WZ4002, erlotinib, crizotinib, a more favorable *in vivo* MET inhibitor (19), or vehicle for 3 days. In particular, imaging studies with ^{18}F-FDG PET/CT were performed in tumor-bearing mice before and after treatment with the efficient inhibitor or

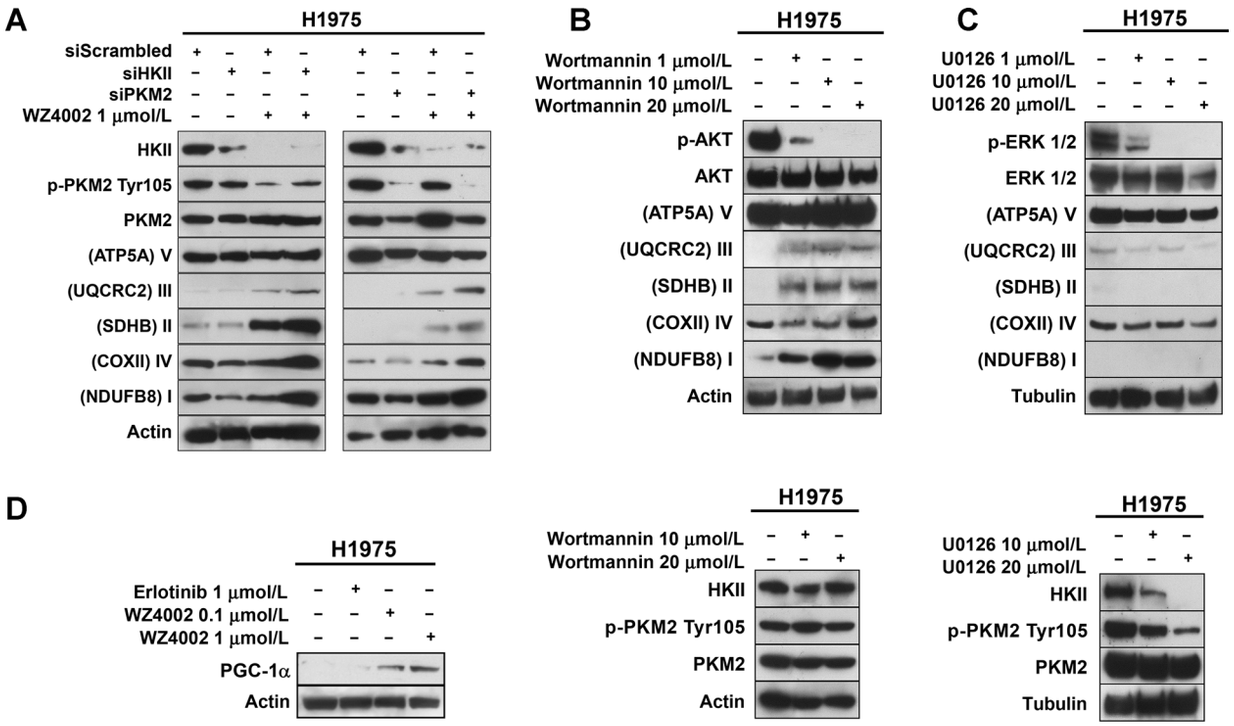

Figure 5.
HKII and PKM2 silencing and selective inhibition of ERK1/2 and AKT pathways. A, H1975 cells were transfected with HKII or PKM2 targeted siRNA pools and control nontargeting siRNA pool (scrambled). After 24 hours, cells were treated with 1 μmol/L WZ4002 or vehicle for 48 hours and then lysed. Levels of HKII, p-PKM2 Tyr105, total PKM2, and OXPHOS were determined by Western blot analysis. B, H1975 cells were treated with increasing concentration of the AKT inhibitor wortmannin or (C) ERK1/2 inhibitor U0126 for 48 hours. Then levels of HKII, p-PKM2 Try105, total PKM2, and OXPHOS were assessed by Western blot analysis. D, levels of PGC-1α were determined in H1975 cells in response to 48 hours treatment with erlotinib or WZ4002. Actin or tubulin served to ensure equal loading.

vehicle. Representative images of ^{18}F-FDG PET/CT studies are shown in Fig. 6A and B. A decrease of ^{18}F-FDG uptake in tumors was found in posttreatment scans of all H1975 and H1993 tumor-bearing mice treated with WZ4002 and crizotinib, respectively. Conversely, an increased tracer uptake was observed in control animals. After treatment and imaging studies, tumors were surgically removed, homogenized and tested for levels of HKII, p-PKM2 Tyr105, total PKM2, and OXPHOS by Western blot analysis (Fig. 6C). In agreement with *in vitro* findings, a dramatic reduction of HKII and p-PKM2 levels along with a strong upregulation of OXPHOS (subunits I-IV) was found in H1975 and H1993 tumors from animals treated with WZ4002 or crizotinib, respectively, as compared with vehicle-treated controls. Interestingly, a slight increase of OXPHOS was also found in animals bearing H1993 xenografts treated with erlotinib. These findings indicate that reactivation of oxidative phosphorylation can occur *in vivo* at drug concentration achievable in the plasma of treated animals bearing NSCLC with mutated or wild-type EGFR.

Discussion

We report that effective inhibition of EGFR signaling downregulates aerobic glycolysis and restores oxidative phosphorylation in NSCLC cell lines and animal tumor models through the concerted downregulation of HKII and p-PKM2 Tyr105 and upregulation of OXPHOS. Furthermore, we provide evidence that selective inhibition of AKT-mediated signaling results in a dose-dependent upregulation of mitochondrial complexes subunits, whereas inhibition of the ERK1/2 pathway causes a reduction of p-PKM2 Tyr105 and HKII levels.

Somatic mutations causing activation of oncogenes or loss of function of tumor-suppressor genes are major determinants of the glycolytic phenotype in cancer cells (8). The maintenance and regulation of this phenotype is under the complex control of a signaling network that is highly dependent on cellular context. In our study, changes of glucose metabolism in response to EGFR signaling inhibition were investigated in the same cellular context represented by erlotinib-resistant NSCLC cells that become sensitive when exposed to EGFR^{T790M} or MET-targeted agents. This approach allowed us to compare the effects of efficient EGFR inhibition on glucose metabolism in three cell lines with a different genetic profile and signaling network status. Despite this diversity, we found that all cell lines share a common response to efficient EGFR inhibition involving the same key proteins of the glycolytic cascade, that is, HKII and p-PKM2 Tyr105. In the absence of genetic alterations of mitochondrial complexes, the inhibition of aerobic glycolysis is accompanied by the reactivation of mitochondrial phosphorylation and by the increase of intracellular ATP production.

High levels of PKM2 are expressed in a variety of human tumors, including lung, breast, and colon cancer (28), and are reported to promote the Warburg effect in cancer cells (5, 6). PKM2 exists as a low-activity dimeric or high-activity tetrameric form and cancer cells predominantly express the low-activity

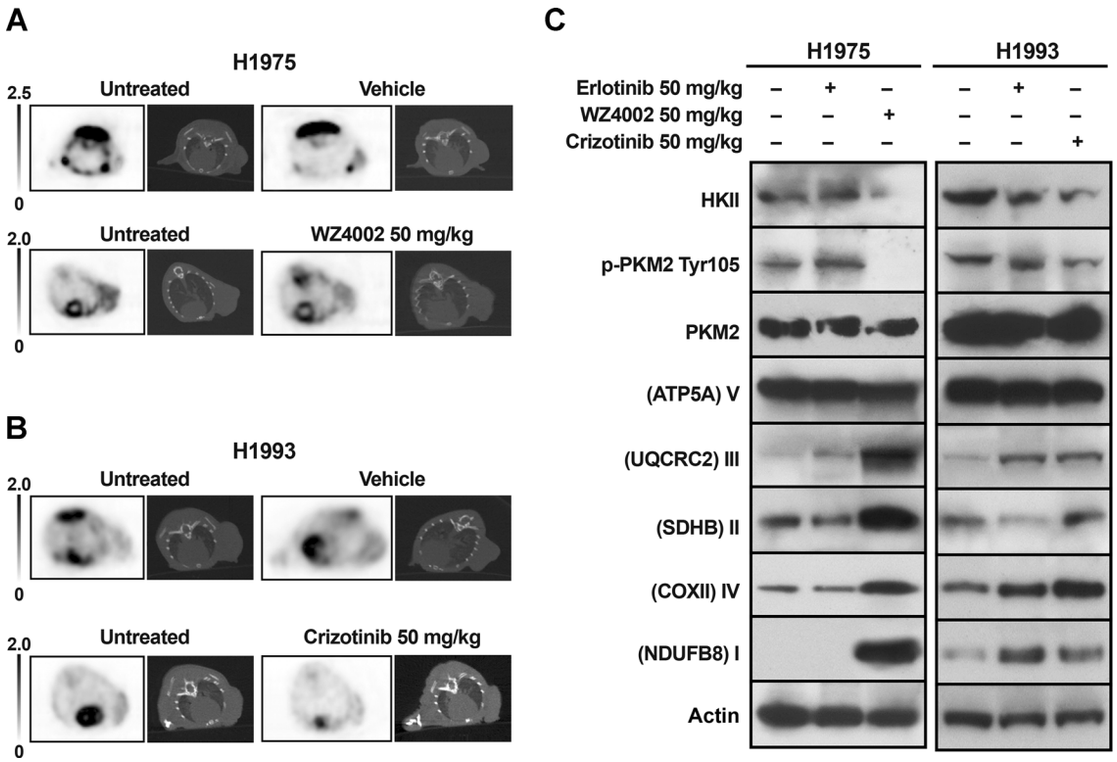

Figure 6.
^{18}F-FDG PET/CT imaging studies and levels of HKII, p-PKM2 Tyr 105, total PKM2, and OXPHOS in tumor xenografts. Nude mice bearing H1975 or H1993 tumors were treated for 3 days by oral gavage with 50 mg/kg of erlotinib, WZ4002, crizotinib or vehicle. A and B, imaging studies with ^{18}F-FDG PET/CT were performed before (left) and after treatment with efficient inhibitor or vehicle (right) of H1975 (A) and H1993 (B) tumors. Representative transaxial ^{18}F-FDG PET and coregistered CT images are shown. C, surgically removed tumors (3 for each cell line and for each treatment) were homogenized and assayed for levels of HKII, p-PKM2 Tyr105, total PKM2, and OXPHOS by Western blot analysis. Actin served to ensure equal loading.

dimeric form with a reduced ability to convert phosphoenolpyruvate to pyruvate (30). Phosphorylation of PKM2 at Tyr105 is reported to disrupt the active tetrameric form (26, 27) and to reduce its catalytic activity. Therefore, the reduction of p-PKM2 Tyr105 levels in response to EGFR inhibitors promotes tetramer formation and a high enzymatic catalytic activity in NSCLC. This state is reported to be associated with efficient ATP generation and catabolic metabolism by redirecting pyruvate flux toward mitochondrial oxidative phosphorylation (31). In agreement with these observations, we showed OXPHOS upregulation and an increase of intracellular ATP following reduction of p-PKM2 Tyr105 levels by EGFR inhibition. The PKM2-dependent downregulation of HKII levels observed in our study may contribute to increase catabolic metabolism by reducing glycolytic intermediates levels and their flux into subsidiary anabolic pathways. A metabolomic analysis in lung adenocarcinoma cells showed indeed that inhibition of EGFR signaling downregulates intermediate metabolites in glycolysis and the pentose phosphate pathway (32).

The abnormally high rate of glucose uptake in cancer cells has been for years the major rationale for the use of ^{18}F-FDG-PET in cancer detection, staging, and treatment monitoring (33). Previous clinical studies with ^{18}F-FDG-PET reported that NSCLC patients who respond to treatment with EGFR TKIs show a prompt reduction of ^{18}F-FDG uptake as early as 48 hours after initiation of treatment (34–36). Such early metabolic response is predictive of morphovolumetric tumor response, progression-free and overall survival. Furthermore, the early reduction of ^{18}F-FDG uptake in EGFR-mutant tumors was reported to be higher (median 55%) than that found in metabolic responding EGFR wild-type tumors (median 19.9%; ref. 36). The rapid reduction of ^{18}F-FDG uptake in response to EGFR TKIs was mainly correlated with the inhibition of the PI3K–AKT pathway, reduction of hexokinase activity, and downregulation of glucose transporters (25). Our findings are in agreement with these observations and provide additional insight into the molecular mechanisms underlying the concerted modulation of aerobic glycolysis and mitochondrial respiration.

Advances in cancer metabolism research increased the clinical interest to target aberrant metabolic pathways for treatment of malignant tumors (37, 38), and a number of compounds interfering with metabolic regulators, enzymes, and metabolic intermediates have been developed (39). Here, we show that EGFR TKIs exert an early and profound effect on aerobic glycolysis and are able to reactivate oxidative phosphorylation. These findings may have relevant clinical implications because EGFR TKIs, in addition to cause growth arrest and apoptosis, may reactivate oxidative phosphorylation and oxygen consumption of cancer cells, which ultimately will improve sensitivity to chemotherapy and radiation therapy. Furthermore, the reduction of lactate secretion may increase extracellular pH, thus improving microenvironmental conditions of cancer cells and response to therapy (40). Also, the differential regulation of aerobic glycolysis and

oxidative phosphorylation by ERK1/2 and AKT pathways, respectively, provides a mechanistic clue for rational combinations of anti-cancer agents targeting EGFR pathways and glucose metabolism exploiting the potential synergistic effects suggested by HKII and PKM2 silencing. In conclusion, our study indicates that innovative therapeutic strategies targeting glucose metabolism may be highly potentiated by the combination with agents targeting the oncogene driver of a given tumor.

Disclosure of Potential Conflicts of Interest

No potential conflicts of interest were disclosed.

Authors' Contributions

Conception and design: V. De Rosa, S. Del Vecchio
Development of methodology: V. De Rosa, F. Iommelli, M. Monti, R. Fonti, G. Votta
Acquisition of data (provided animals, acquired and managed patients, provided facilities, etc.): V. De Rosa, M. Monti, R. Fonti, G. Votta
Analysis and interpretation of data (e.g., statistical analysis, biostatistics, computational analysis): V. De Rosa, F. Iommelli, S. Del Vecchio
Writing, review, and/or revision of the manuscript: V. De Rosa, M.P. Stoppelli, S. Del Vecchio
Administrative, technical, or material support (i.e., reporting or organizing data, constructing databases): S. Del Vecchio
Study supervision: S. Del Vecchio

Grant Support

This work was partly supported by the Ministry of University and Research, MERIT—MEdical Research in Italy (project No. RBNE08YFN3_008) and AIRC, Associazione Italiana per la Ricerca sul Cancro (project no. IG-11756).

The costs of publication of this article were defrayed in part by the payment of page charges. This article must therefore be hereby marked *advertisement* in accordance with 18 U.S.C. Section 1734 solely to indicate this fact.

Received February 13, 2015; revised June 15, 2015; accepted June 19, 2015; published OnlineFirst July 27, 2015.

References

1. Cairns RA, Harris IS, Mak TW. Regulation of cancer cell metabolism. Nat Rev Cancer 2011;11:85–95.
2. Cantor JR, Sabatini DM. Cancer cell metabolism: one hallmark, many faces. Cancer Discov 2012;2:881–98.
3. Warburg O. On respiratory impairment in cancer cells. Science 1956;124:269–70.
4. Warburg O. On the origin of cancer cells. Science 1956;123:309–14.
5. Vander Heiden MG, Cantley LC, Thompson CB. Understanding the Warburg effect: the metabolic requirements of cell proliferation. Science 2009;324:1029–33.
6. Christofk HR, Vander Heiden MG, Harris MH, Ramanathan A, Gerszten RE, Wei R, et al. The M2 splice isoform of pyruvate kinase is important for cancer metabolism and tumour growth. Nature 2008;452:230–3.
7. Levine AJ, Puzio-Kuter AM. The control of the metabolic switch in cancers by oncogenes and tumor suppressor genes. Science 2010;330:1340–4.
8. Ward PS, Thompson CB. Metabolic reprogramming: a cancer hallmark even Warburg did not anticipate. Cancer Cell 2012;21:297–308.
9. Yang W, Zheng Y, Xia Y, Ji H, Chen X, Guo F, et al. ERK1/2-dependent phosphorylation and nuclear translocation of PKM2 promotes the Warburg effect. Nat Cell Biol 2012;14:1295–304.
10. Pao W, Chmielecki J. Rational, biologically based treatment of EGFR-mutant non–small cell lung cancer. Nat Rev Cancer 2010;10:760–74.
11. Lynch TJ, Bell DW, Sordella R, Gurubhagavatula S, Okimoto RA, Brannigan BW, et al. Activating mutations in the epidermal growth factor receptor underlying responsiveness of non–small cell lung cancer to gefitinib. N Engl J Med 2004;350:2129–39.
12. Paez JG, Janne PA, Lee JC, Tracy S, Greulich H, Gabriel S, et al. EGFR mutations in lung cancer: correlation with clinical response to gefitinib therapy. Science 2004;304:1497–500.
13. Pao W, Miller V, Zakowski M, Doherty J, Politi K, Sarkaria I, et al. EGF receptor gene mutations are common in lung cancers from "never smokers" and are associated with sensitivity of tumors to gefitinib and erlotinib. Proc Natl Acad Sci U S A 2004;101:13306–11.
14. Sequist LV, Martins RG, Spigel D, Grunberg SM, Spira A, Janne PA, et al. First-line gefitinib in patients with advanced non–small cell lung cancer harboring somatic EGFR mutations. J Clin Oncol 2008;26:2442–9.
15. Pao W, Miller VA, Politi KA, Riely GJ, Somwar R, Zakowski MF, et al. Acquired resistance of lung adenocarcinomas to gefitinib or erlotinib is associated with a second mutation in the EGFR kinase domain. PLoS Med 2005;2:e73.
16. Kobayashi S, Boggon TJ, Dayaram T, Janne PA, Kocher O, Meyerson M, et al. EGFR mutation and resistance of non–small cell lung cancer to gefitinib. N Engl J Med 2005;352:786–92.
17. Engelman JA, Zejnullahu K, Mitsudomi T, Song Y, Hyland C, Park JO, et al. MET amplification leads to gefitinib resistance in lung cancer by activating ERBB3 signaling. Science 2007;316:1039–43.
18. Zannetti A, Iommelli F, Speranza A, Salvatore M, Del Vecchio S. 3′-deoxy-3′-18F-fluorothymidine PET/CT to guide therapy with epidermal growth factor receptor antagonists and Bcl-xL inhibitors in non–small cell lung cancer. J Nucl Med 2012;53:443–50.
19. Iommelli F, De Rosa V, Gargiulo S, Panico M, Monti M, Greco A, et al. Monitoring reversal of MET-mediated resistance to EGFR tyrosine kinase inhibitors in non–small cell lung cancer using 3′-deoxy-3′-[18F]-fluorothymidine positron emission tomography. Clin Cancer Res 2014;20:4806–15.
20. Ohashi K, Maruvka YE, Michor F, Pao W. Epidermal growth factor receptor tyrosine kinase inhibitor-resistant disease. J Clin Oncol 2013;31:1070–80.
21. Sharma SV, Bell DW, Settleman J, Haber DA. Epidermal growth factor receptor mutations in lung cancer. Nat Rev Cancer 2007;7:169–81.
22. Kubo T, Yamamoto H, Lockwood WW, Valencia I, Soh J, Peyton M, et al. MET gene amplification or EGFR mutation activate MET in lung cancers untreated with EGFR tyrosine kinase inhibitors. Int J Cancer 2009;124:1778–84.
23. Zhao X, Weir BA, LaFramboise T, Lin M, Beroukhim R, Garraway L, et al. Homozygous deletions and chromosome amplifications in human lung carcinomas revealed by single nucleotide polymorphism array analysis. Cancer Res 2005;65:5561–70.
24. Zannetti A, Iommelli F, Fonti R, Papaccioli A, Sommella J, Lettieri A, et al. Gefitinib induction of *in vivo* detectable signals by Bcl-2/Bcl-xL modulation of inositol trisphosphate receptor type 3. Clin Cancer Res 2008;14:5209–19.
25. Su H, Bodenstein C, Dumont RA, Seimbille Y, Dubinett S, Phelps ME, et al. Monitoring tumor glucose utilization by positron emission tomography for the prediction of treatment response to epidermal growth factor receptor kinase inhibitors. Clin Cancer Res 2006;12:5659–67.
26. Christofk HR, Vander Heiden MG, Wu N, Asara JM, Cantley LC. Pyruvate kinase M2 is a phosphotyrosine-binding protein. Nature 2008;452:181–6.
27. Hitosugi T, Kang S, Vander Heiden MG, Chung TW, Elf S, Lythgoe K, et al. Tyrosine phosphorylation inhibits PKM2 to promote the Warburg effect and tumor growth. Sci Signal 2009;2:ra73.
28. Luo W, Semenza GL. Emerging roles of PKM2 in cell metabolism and cancer progression. Trends Endocrinol Metab 2012;23:560–6.
29. Birsoy K, Possemato R, Lorbeer FK, Bayraktar EC, Thiru P, Yucel B, et al. Metabolic determinants of cancer cell sensitivity to glucose limitation and biguanides. Nature 2014;508:108–12.
30. Mazurek S. Pyruvate kinase type M2: a key regulator of the metabolic budget system in tumor cells. Int J Biochem Cell Biol 2011;43:969–80.
31. Anastasiou D, Yu Y, Israelsen WJ, Jiang JK, Boxer MB, Hong BS, et al. Pyruvate kinase M2 activators promote tetramer formation and suppress tumorigenesis. Nat Chem Biol 2012;8:839–47.
32. Makinoshima H, Takita M, Matsumoto S, Yagishita A, Owada S, Esumi H, et al. Epidermal growth factor receptor (EGFR) signaling regulates global

metabolic pathways in EGFR-mutated lung adenocarcinoma. J Biol Chem 2014;289:20813–23.
33. Plathow C, Weber WA. Tumor cell metabolism imaging. J Nucl Med 2008;49:43S-63S.
34. Zander T, Scheffler M, Nogova L, Kobe C, Engel-Riedel W, Hellmich M, et al. Early prediction of nonprogression in advanced non–small cell lung cancer treated with erlotinib by using [(18)F]fluorodeoxyglucose and [(18)F]fluorothymidine positron emission tomography. J Clin Oncol 2011;29:1701–8.
35. Takahashi R, Hirata H, Tachibana I, Shimosegawa E, Inoue A, Nagatomo I, et al. Early [18F]fluorodeoxyglucose positron emission tomography at two days of gefitinib treatment predicts clinical outcome in patients with adenocarcinoma of the lung. Clin Cancer Res 2012;18:220–8.
36. Mileshkin L, Hicks RJ, Hughes BG, Mitchell PL, Charu V, Gitlitz BJ, et al. Changes in 18F-fluorodeoxyglucose and 18F-fluorodeoxythymidine positron emission tomography imaging in patients with non–small cell lung cancer treated with erlotinib. Clin Cancer Res 2011;17:3304–15.
37. Tennant DA, Duran RV, Gottlieb E. Targeting metabolic transformation for cancer therapy. Nat Rev Cancer 2010;10:267–77.
38. Teicher BA, Linehan WM, Helman LJ. Targeting cancer metabolism. Clin Cancer Res 2012;18:5537–45.
39. Vander Heiden MG. Targeting cancer metabolism: a therapeutic window opens. Nat Rev Drug Discov 2011;10:671–84.
40. Hsu PP, Sabatini DM. Cancer cell metabolism: Warburg and beyond. Cell 2008;134:703–7.